IEEE Access
Multidisciplinary | Rapid Review | Open Access Journal

Received July 24, 2021, accepted September 10, 2021, date of publication September 14, 2021, date of current version September 21, 2021.

Digital Object Identifier 10.1109/ACCESS.2021.3112390

Development of a Far-Field Noise Estimation Model for an Aircraft Auxiliary Power Unit

UMAIR AHMED, FAKHRE ALI, AND IAN K. JENNIONS
Integrated Vehicle Health Management Centre, School of Aerospace, Transport and Manufacturing, Cranfield University, Bedfordshire MK43 0AL, U.K.
Corresponding author: Umair Ahmed (umair.ahmed@cranfield.ac.uk)

This work was supported by The Boeing Company.

ABSTRACT Aircraft Auxiliary Power Unit (APU) is one of the major aircraft systems and is reported to be a key driver of unscheduled maintenance. So far, the research has been focused on the implementation of the APU thermodynamic state data to isolate and diagnose faults. To advance the available diagnostic techniques, research work has been initiated to explore the potential of employing far-field microphone data for the identification and isolation of APU faults. This paper aims to address the first step required in the overall effort and proposes a novel methodology for the development of a noise model that can be used for evaluating noise as a source of fault diagnostics. The methodology integrates experimentally acquired full-scale aircraft state and noise data, a physics-based APU thermodynamic model, and semi-empirical noise models to estimate the noise produced by an aircraft APU based on a limited parameter-set. The methodology leads to a model which works by estimating the unknown thermodynamic parameters from the limited dataset and then passes on the relevant parameters to noise estimation models (combustion/jet noise models). An inherent part of the model is the effect of multipath propagation and ground reflections for which a relationship has been analytically derived that considers all the necessary parameters. The developed model has been validated against experimental noise and thermodynamic data acquired from a Boeing 737-400 aircraft APU under several different operating conditions. The acquired noise estimates suggest that the proposed approach provides an accurate estimation of the far-field noise under a wide range of APU operating conditions, both at the sub-system and APU level. The model would act as an enabler to simulate APU noise data under degraded functional states and subsequently developing fault diagnostic schemes based on the far-field noise data.

INDEX TERMS Acoustic measurements, acoustic noise, acoustic propagation, acoustic signal processing, aircraft, aerospace components, combustion, jet, thermodynamics.

I. INTRODUCTION

The aircraft is a highly complex and integrated system. Amongst, others, one of its major systems, the Auxiliary Power Unit (APU), has been reported as a key driver of unscheduled maintenance and therefore demands a robust maintenance strategy [1]. The heart of maintenance and troubleshooting is a fault diagnostic scheme that comprises a sensor-set and a fault diagnostic algorithm. Generally, a diagnostic capability is embedded into the system during the design phase depending on the technologies (hardware, sensors, processing techniques) available at that time. Performance-based monitoring (also called gas-path analysis) is an example of the prevalent approach for a gas turbine's health monitoring or fault detection [1]–[7]. However, these methods require the installation of thermodynamic sensors which could be intrusive and may not be feasible if they were not considered during the product's design phase. Moreover, with the increasing demand for air travel, the desire to reduce aircraft downtime, and the technological advancements made in the relevant fields, the need for state-of-the-art fault diagnostic solutions is increasing. The proposed solutions should be readily deployable and assist in expediting the unscheduled maintenance activities.

In addition to the thermodynamic parameters, the noise generated by an aircraft APU may also contain useful information about the state of the system and, therefore, assist in detecting degradation or faults. To proceed with the

The associate editor coordinating the review of this manuscript and approving it for publication was Dominik Strzalka.

This work is licensed under a Creative Commons Attribution 4.0 License. For more information, see https://creativecommons.org/licenses/by/4.0/

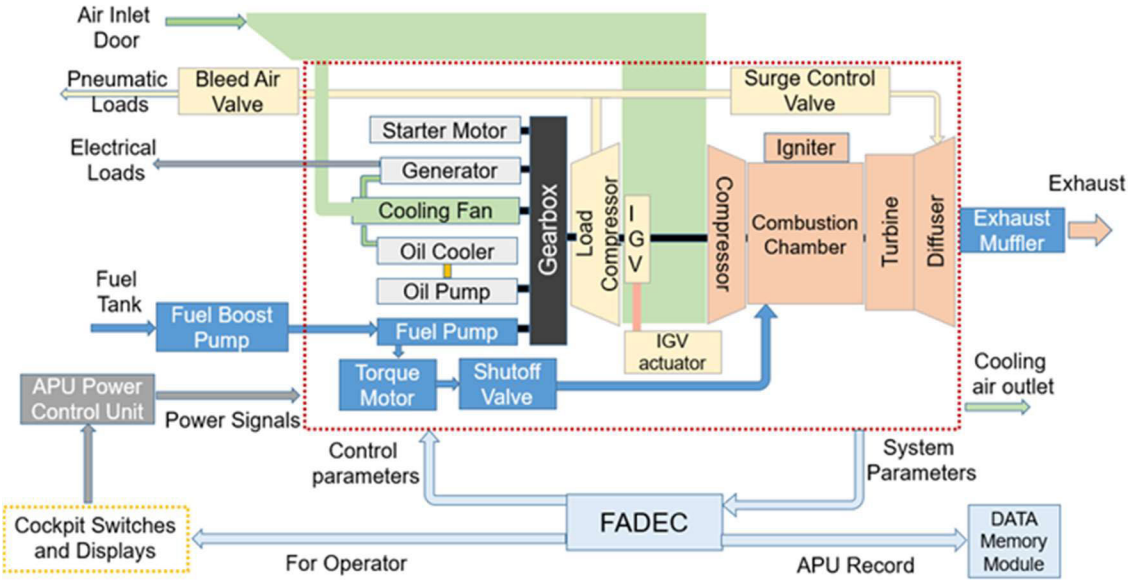

FIGURE 1. Schematics of the adopted APU.

assessment of the noise generated by the aircraft APU as a source of fault diagnostics, a noise estimation model is required. Such a model has been found to be missing from the literature. In this regard, research is being undertaken on a Boeing 737 (B737) aircraft to evaluate the noise radiated by its APU as an enabler for fault diagnostics. In this paper, the focus is on the development of a far-field noise estimation model that would facilitate the characterization of noise when the APU is subjected to faults under various degradation severities.

Various types of experimentation which have been performed on APU have either been focussed on its thermodynamics aspects or the qualitative assessment of its far-field noise. Generally, a test rig is developed to gather information about thermodynamic parameters, acoustics, or exhaust emissions. Several test rigs [1]–[4] have been developed to understand the thermodynamic aspects of APUs. In other forms of experimental data collection, APUs are placed inside an anechoic chamber and their exhaust noise is studied with far-field microphones [5]–[7]. These studies discussed the spectrum of combustion noise and the presence of indirect combustion noise. Another form of experimentation involves the development and testing of noise suppression mechanisms for aircraft APUs [8]. Other studies [9]–[11] have ascertained the average acoustic levels to which the service personnel is exposed while working on the aircraft. Towards the development of noise models for aircraft APUs, very little information is available and is said to be because of the scarcity of APU noise data. A German noise simulation program is reported to be developed for APUs [12], however, its results have not been compared with experimental data and thus its accuracy is questionable.

Contrary to acoustic analysis on APU, extensive work [13]–[18] has been done on turbofan engines, their noise, and the comparison of the performance of various noise estimation models. As per the regulations, the noise from the main engines has to be well within the prescribed limits set by the regulating authorities, which is not the case for aircraft APUs. Therefore, APU noise and its dependence on the underlying physical parameters need to be explored. Recently, we [19] have highlighted that APU far-field noise has not been studied at a full scale and under a wide range of operating conditions. Besides, none of the noise estimation models have been reported to be validated on an aircraft APU using experimental data.

A. DESCRIPTION OF APU

The APU is a gas-turbine engine that is typically installed in the tail section of the aircraft. The APU is responsible for providing pneumatic and electrical power during ground / aerial operations. The APU also serves as a backup source of power during emergencies in flight. APU noise, on the other hand, is an undesired by-product resulting from APU operation. Unlike the main engine, this noise is not regulated by regulating authorities such as the FAA (Federal Aviation Authority), however, it is of major concern for personnel working around the aircraft, as well as from the point of view of noise pollution at the airport terminal. Therefore, local authorities at the airport may restrict the duration of its operation [6].

This study is conducted on Cranfield University's B737-400 aircraft APU which is a turboshaft engine (high-level schematic presented in Fig. 1). The power section of the APU consists of a single-stage centrifugal compressor with 17 impellers, a reverse flow annular combustor, and a radial inflow turbine having 14 blades. The compressor and turbine are mounted on the same shaft which rotates at a constant speed of 63830 rpm for all operating and loading conditions.

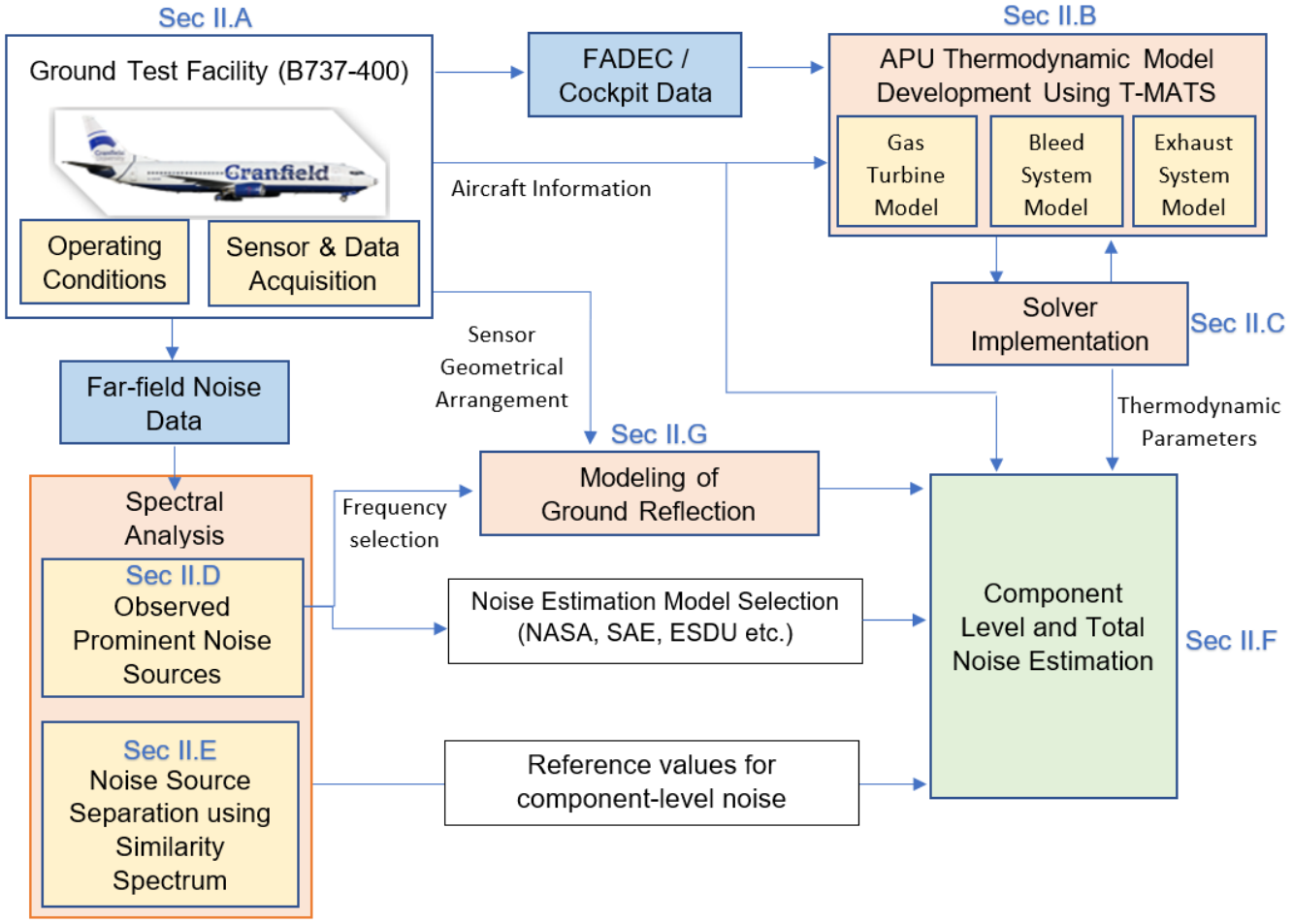

FIGURE 2. Far-field noise model development methodology for an aircraft APU.

The APU shaft also rotates a load compressor which generates pressurized air for the aircraft pneumatic system as per the demand. The bleed air from the APU is delivered to the Environmental Control System (ECS), wing anti-ice system, or to the pneumatic starter of the main engines. A set of inlet guide vanes (IGV) control the amount of air entering the load compressor and hence to the pneumatic system. During the initial phases of start-up, the IGV remains closed but is then allowed to open by 22° to prevent compressor surge. The surge control valve (SCV) is another important component of the APU's pneumatic system. The SCV is controlled by the surge valve torque motor (SVTM) and allows the pressurized air from the load compressor to be rejected into the exhaust system to avoid compressor surges. The overall operation of the APU is controlled by a Full Authority Digital Engine Controller (FADEC) which is installed in the cargo compartment. This unit monitors the state of the system and generates commands for the fuel torque motor, SVTM, and IGV actuator.

B. SCOPE OF WORK

The focus of this paper is on the development of the far-field noise estimation model for an aircraft APU. At the heart of this model are the thermodynamic principles which govern the operation of a gas turbine and allows computation of the unknown thermodynamic parameters. The results are then coupled with appropriate component-level semi-empirical noise estimation relationships. The effect of ground reflections is analytically derived and embedded in the model. The overall model is developed in MATLAB's Simulink environment by using the approach described in Section II. The model's accuracy will be ascertained using the experimentally acquired dataset (Section III). The overall approach allows the rapid development of a robust model that can accurately estimate the far-field noise under a wide range of operating conditions. It can be further enhanced to perform fault injection in APU components, modelling transient response, and component-level noise sensitivity analyses.

II. PROPOSED METHODOLOGY

The methodology for the development of a far-field noise estimation model is presented in Fig. 2. This is a novel approach that systematically considers all necessary aspects of the far-field noise under a wide range of operating conditions. The process begins with the acquisition of far-field noise and thermodynamic data from the aircraft APU. The latter

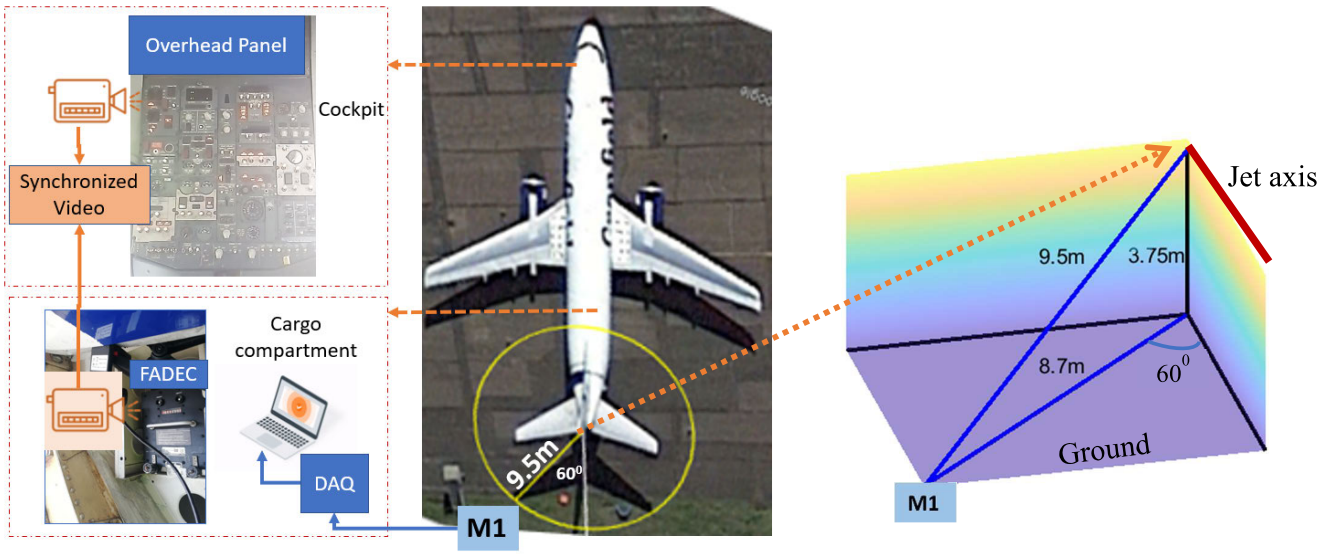

FIGURE 3. Acquisition of experimental data from Boeing 737-400 auxiliary power unit.

is processed using a custom-built thermodynamic model for estimating the unknown parameters. The model is build using Toolbox for the Modelling and Analysis of Thermodynamic Systems (T-MATS), which operates in MATLAB's Simulink environment. In parallel, frequency domain analysis is carried out on the noise data for identifying the prominent sources, enabling the selection of the appropriate noise models. Source separation technique using similarity spectrum is then applied to separate the component-level noise from the experimental far-field noise data. The acquired, separated noise levels serve as the reference values for the noise estimation models. Subsequently, component-level noise estimation models are implemented, which take thermodynamic parameters as input while also accounting for the effect of ground reflections. Eventually, the deviation between the estimated component-level noise and the reference values is determined in order to estimate the total noise. In the subsequent paragraphs, a detailed description of the individual sections of the methodology is elaborated.

A. EXPERIMENTAL SETUP

The overall arrangement for acquiring the necessary data is depicted in Fig. 3. The acoustic data is collected by a 130F20 4" microphone (M1) and is relayed to the Data Acquisition (DAQ) using the NI Integrated Electronics Piezo-Electric (IEPE) module. M1 is at a radial distance of 9.5m and is placed on the concrete taxiway. The figure also shows 3D arrangement of the sensor with respect to the jet axis. The position of the sensor is at an angle of 60° from the jet axes and is selected because it has been reported that the noise from gas-turbine engines has maximum directivity around this angle [20], [21]. Furthermore, the microphone is placed on the left side of the fuselage so that the inlet noise (if any) is masked by the fuselage structure. The microphone is covered with a windscreen to reduce the effects of wind on acoustic measurement. In addition to the sensor, two cameras are installed in the aircraft (see Fig. 3). One camera is placed in the cargo compartment, which records the thermodynamic parameters presented by the FADEC display. This display conveys information about the rpm, inlet pressure/temperature, EGT, and positions of IGV / SCV. Another camera monitors the activities inside the cockpit. The videos from both sources are timestamped for synchronization. During one of the test runs, a thermocouple was held at the exhaust to measure the temperature at the exit of the exhaust muffler.

The methodology requires data collection under a wide range of APU operating conditions. For the successful implementation of this study, the overall data is acquired at 8 different APU operating conditions (C1, C2,....C8), and is repeated for 8 different days, resulting in a total of 64 datasets (see Fig. 4). The test conditions represent various combinations of electrical and pneumatic load, some conditions have been intentionally duplicated (for example C4 and C7, both correspond to bleed on with no load). This is done so that any variation in the parameters due to the prolonged duration of APU operation can be captured within the data collection. For example, C2 and C8 are both no-load conditions (Bleed off and 0A electrical load), however, a slight change in oil temperatures is present between these two conditions, which can have a very small effect on the fuel consumption at these two conditions. Furthermore, by increasing the number of data points, a certain trend in the unknown parameters can also be ascertained. Data collected at a particular condition on a specific day will be termed as a Dataset (for example 1,9,17...represent the data collected on day 1). At each dataset, part of the thermodynamic parameters (observable through the FADEC) is acquired. With regards to

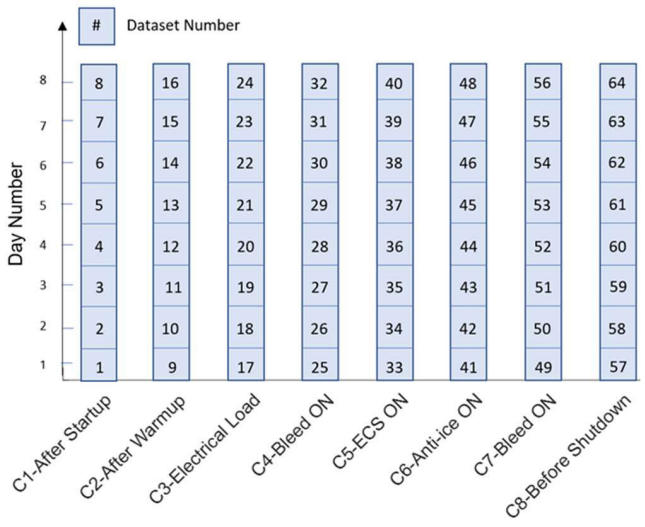

FIGURE 4. APU operating conditions and representation of experimental datasets.

the microphone data, a one-second interval is selected that is converted into SPL values (termed as $SPL_{Measured}$). All the values of the dataset at a given operating condition will be accumulated for boxplot analysis and for observing the overall trend in the data. However, the values at the dataset level will be used to compare the accuracy of the noise estimation model.

B. APU THERMODYNAMIC MODEL DEVELOPMENT

The onboard APU FADEC display provides limited technical data (e.g. thermodynamic data) to efficiently support the implementation of the adopted empirical noise estimation models. Therefore, a customized gas turbine simulation model is developed using Toolbox for the Modelling and Analysis of Thermodynamic Systems (T-MATS) turbomachinery components (compressor, turbine, shaft, and a burner) (see Fig. 5). The symbols used in this paper are listed in Table-1.

T-MATS is an open-source Simulink-based plugin developed by NASA Glenn Research Centre, which can be utilized by industry personnel or academics without any restrictions. T-MATS allows the development of a customized gas turbine using modular turbomachinery components, which can be analyzed in detail by integrating the model with the software-provided iterative solvers. The research community has frequently used T-MATS for simulating the performance of gas turbines ([1], [22], and [23] are some of the examples), but it has not been adopted for noise modelling purposes.

Since T-MATS is a Simulink-based platform, it allows customized code to be integrated to compute other parameters as per the requirements and to execute the model under different operating conditions. The T-MATS component blocks can be altered to execute in the absence of performance maps that are proprietary to the manufacturer. The thermodynamic model is the core part of the overall methodology and mimics the behaviour of various sections of the APU, that can influence the far-field noise. So, customized code is integrated with the T-MATS blocks to model the Surge Control Valve, Mixer, and Exhaust Muffler.

To simplify the model, the following assumptions have been made:

1) The compressor and turbine (mounted on the same shaft) have the same pressure ratio under all operating conditions and are assumed to be equal to the maximum pressure ratio acquired through FADEC corresponding to the load compressor.
2) Mixing is adiabatic at the mixer and the muffler.
3) The compressor and turbine operate on a similar isentropic efficiency for a given operating condition. The load compressor efficiency ($Eff_{Load\ Compressor}$) is assumed to be proportional to the IGV position.
4) The changes in the air temperature downstream of the surge valve are negligible.
5) The surge control valve linearly controls the mass flow as a function of SVTM current ($\dot{m}SV \propto ISVTM$), acquired from the FADEC readings.

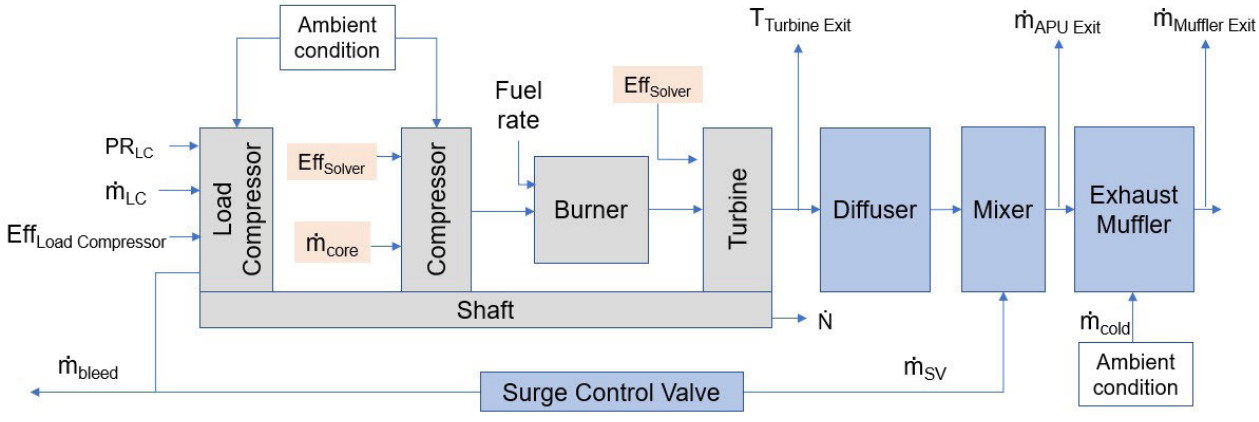

FIGURE 5. APU model developed in T-MATS.

TABLE 1. Symbols used and their description.

Symbol	Description
A_b	Buner cross-sectional area
A_{jet}	Muffler cross-sectional area
c_0	Speed of sound in ambient condition
$c_{C/Jet-Model}$	Offset computed for Combustion/Jet Model
c_p	specific heat at constant pressure
c_{refl}	Sound reflection coefficient
DI	Directivity Index
$Djet$	Exhaust jet diameter
$Eff_{Load\ Compressor}$	Load compressor efficiency
Eff_{Solver}	Component efficiency computed by solver
F_b	Burner fuel to air ratio
F_{st}	Stochiometric fuel to air ratio
H_f	Fuel heating value
$\dot{m}_{core}$	Mass flow through the engine core
$\dot{m}_{bleed}$	Mass flow through aircraft bleed system
$\dot{m}_{LC}$	Mass flow generated by load compressor
$\dot{m}_{SV}$	Mass flow through the surge control valve
$\dot{m}_{APU\ Exit}$	Mass flow exiting the APU
$\dot{m}_{cold}$	Mass flow entering the muffler
$\dot{m}_{Muffler\ Exit}$	Mass flow exiting the muffler
$\dot{N}$	Rate of change of rotor rpm
N_f	Number of fuel nozzles
ρ_{Jet}	Jet density
PR_{LC}	Pressure Ratio for Load Compressor
P_{Amb}	Ambient Pressure
$P_{Turbine\ Inlet}$	Combustor exit total pressure
P_3	Combustor inlet total pressure
$Q_{Combustion}$	Combustion noise propagation coefficient
Q_{Jet}	Jet noise propagation coefficient
R	Universal gas constant
r	The radial distance between APU exhaust and sensor M1
$SPL^{Basic}_{C/Jet-Model}$	SPL computed by the original form of Combustion / Jet noise model
$SPL_{C\text{-}model\text{-}i}$	Combustion noise estimated by Model i
$SPL_{Jet\ model\ i}$	Jet noise estimated by Model i
$SPL_{Measured}$	SPL of the far-field noise measured at M1
T_{Amb}	Ambient temperature
T_{Jet}	Jet temperature
$T_{Turbine\ Exit}$	Exhaust Gas Temperature
$T_{Turbine\ Inlet}$	Turbine inlet temperature
T_3	Combustor inlet temperature
v_{jet}	Jet velocity

6) For Muffler, the value for $\dot{m}_{Cold}$ is a factor (F) of $\dot{m}_{APU\ Exit}$, such that the exit temperature matches the measured muffler exit temperature. This approach is based on the work performed in [24].
7) The total pressure at the muffler and diffuser exit is equal to ambient conditions.
8) The efficiency of the electrical generator is chosen to be 95%, whereas for the burner it is assumed to be 99% (supported by ([25] and [26])

C. SOLVER IMPLEMENTATION

This section will explain the process by which the unknown engine parameters are estimated using the T-MATS provided solver. At each operating condition, the parameters of the APU model are updated using experimental test data. The T-MATS solver is then implemented to iteratively update core mass flow, and component efficiencies in order to meet the following set of conditions (see Fig. 6):

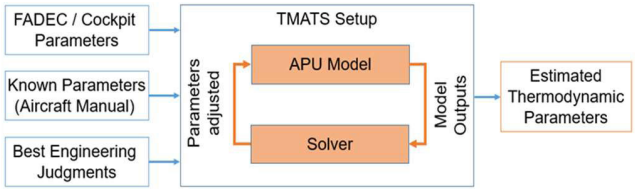

FIGURE 6. Thermodynamic parameter estimation using T-MATS.

1) The computed EGT at the turbine outlet is equal to the value measured by the FADEC. Meeting this condition ensures that the solver meets the experimentally determined value for the EGT.
2) The total pressure at the output of the diffuser should be equal to the ambient pressure.
3) The net torque on the shaft is zero, which means that the torque produced by the turbine equals the sum of torques required by the compressors and the generator. This condition leads to no change in the rpm ($\dot{N} = 0$).

D. SPECTRAL ANALYSIS OF FAR-FIELD NOISE

This study identifies the optimum combination of noise models that can provide acceptable levels of accuracy for far-field noise estimation from an APU. Combustion (or core) noise models and jet noise models are considered since the combination of these two models provided meaningful results. The compressor noise generally propagates towards the inlet which is not the focus of this study. Moreover, compressor blade pass frequency is not present in the far-field noise spectra. Noise is also generated by the turbine, but it is assumed that it is attenuated by the exhaust muffler to an extent that it is overwhelmed by the broadband jet noise. This has been experimentally verified by observing the frequency content of the acquired far-field data [Figure 7(a) (frequency spectrum in blue colour) shows the non-existence of prominent noise around the turbine blade pass frequency of 14.89kHz].

E. NOISE SOURCE SEPARATION USING SIMILARITY SPECTRUM

This section focuses on describing the methodology that has been adopted in separating the noise sources from

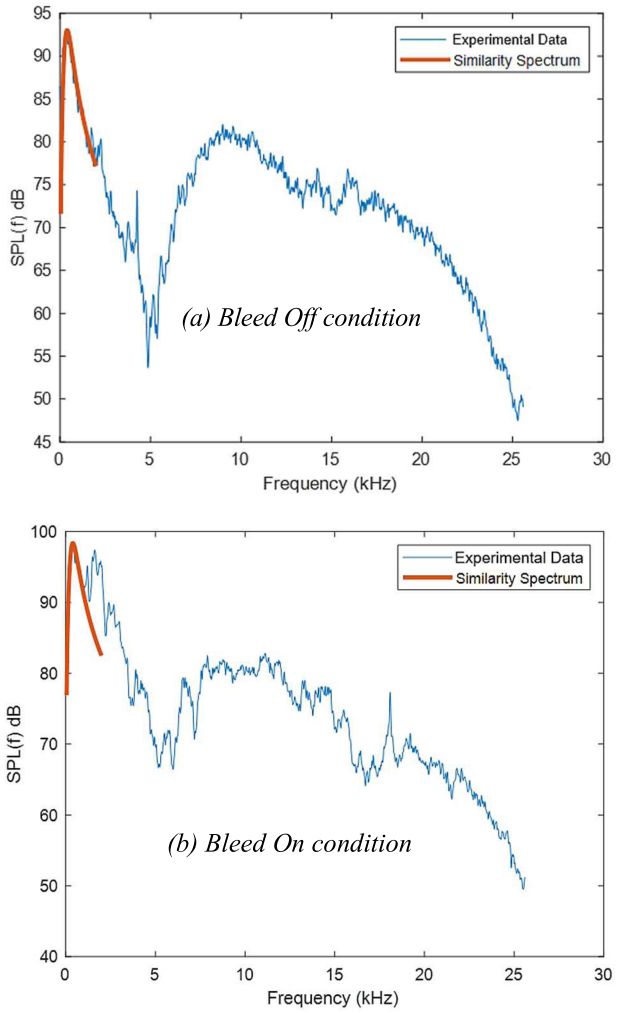

FIGURE 7. Power spectrum of far-field acoustic data with similarity spectrum superimposed.

experimental data. The approach relies on the assumption that the far-field noise from the APU consists of combustion and jet noise only. With this assumption, spectral analysis has been carried out on the raw data. Initially, power spectrum $S(f)$ is acquired using MATLAB's *pspectrum* function, which is then converted in SPL values using the following relationship:

$$SPL\,(f) = 20\log\left[\frac{S\,(f)}{20x10^{-6}}\right] \tag{1}$$

The power spectrum is then compared with the similarity spectrum which has been specified to be the characteristic of combustion noise. This spectrum has been reported in the literature [21], [27] and shown to be significantly contributing towards the overall noise at low frequencies (<2kHz). As per [21], the spectral shape [$SS\,(f)$] can be reproduced by using the following relationship:

$$SS\,(f) = -16\log\left[(0.003037f)^{1.8509} + (0.002051f)^{-1.8168}\right] \tag{2}$$

An offset value is then computed that would reduce the mean difference between SPL(f) and SS(f) for frequencies less than 2kHz. The complete process would lead to a situation depicted in figure 7(a) which shows the power spectrum of far-field acoustic data from APU in bleed-off condition with the similarity spectrum superimposed on it. The same process is shown for the bleed on condition and the results are shown in figure 7(b).

From this analysis, combustion noise is estimated to be equal to the power contained in the similarity spectra if it is lower or equal to the spectral power of the acoustic data in the same frequency range. If the similarity spectrum becomes greater, only the power inside the raw acoustic data is taken. For computing the power, MATLAB's *pwelch* function is used which can provide the spectral power for a given range of frequencies [28]:

$$P_{1,2} = \int_{f1}^{f2} P_{yy}\,(f)\,df \approx \sum_{i1}^{i2} P_{yy}\,[i] \tag{3}$$

where, P_{yy} is the frequency transform computed using *pwelch* function and i1 and i2 are the indexes of frequencies related to the combustion noise. $P_{1,2}$ is the RMS value of the required combustion noise. The remaining part of the noise (assumed to be the jet noise) is computed by subtracting the combustion noise from the total power contained in the acoustic signal. The complete process will be performed for all 64 instances and the results will be presented in Section III. The noise sources separated in this manner will be termed as $SPL^{experimental}_{Jet(i)}$ and $SPL^{experimental}_{Combustion(i)}$, where '$i$' is the dataset number at which they are calculated.

F. COMPONENT LEVEL NOISE ESTIMATION MODEL IMPLEMENTATION

Various noise estimation models are available which can estimate noise generated at the component level or by treating the gas turbine as a single component. These models can range from empirical / semi-empirical relationships to more complex physics-based numerical solutions. The latter approach is time-consuming, bears a high computational cost, and demands a detailed level of system design and geometry parameters, these are generally propriety information limited to the manufacturer only. On the other hand, the semi-empirical relationships provide a rapid computation of noise parameters from engine components based on thermodynamic and geometric parameters. These models are continuously evolving and being updated based on the acquired experimental data, however, specifically in the case of APU, they have not been reported to be validated against the actual aircraft data under various load conditions. As per the spectral analysis, combustion and jet noise are the major constituents in the experimentally acquired far-field noise. Therefore, only these two components will be estimated by adopting two different models.

1) JET NOISE ESTIMATION MODELS

For jet noise estimation, the Engineering Sciences Data Unit (ESDU) model has been utilized because it is said to be valid for lower jet velocities, as in the case of an APU. The acoustic power is proportional to the jet density, velocity, and diameter, and is given by [29],

$$W_{Jet} \propto \frac{\rho_{Jet} v_{Jet}^8 D_{Jet}^2}{c_0^5} \tag{4}$$

This relationship incorporates the core variables on which the jet noise power is dependent. However, information about the proportionality constant and the Directivity Index is not provided in [29]. In order to convert W_{Jet} into SPL_{Jet} at a particular angle θ and distance 'r' Eq.4 would become,

a: JET MODEL 1

$$\begin{aligned} SPL_{Jet-Model-1} &= 10\log\left[\frac{K_{Jet-model-1}^{empirical}\rho_{Jet} v_{Jet}^8 D_{Jet}^2}{c_0^5 10^{-12}}\right] \\ &+10\log\left[\frac{Q_{Jet}}{4\pi r^2}\right] + DI(\theta) \end{aligned}$$

Or,

$$\begin{aligned} SPL_{Jet-Model-1} &= 10\log\left[\frac{\rho_{Jet} v_{Jet}^8 D_{Jet}^2}{c_0^5 10^{-12}}\right] \\ &+10\log\left[\frac{Q_{Jet}}{4\pi r^2}\right] \\ &+10\log\left[K_{Jet-model-1}^{empirical}\right] + DI(\theta) \end{aligned} \tag{5}$$

Let,

$$\theta c_{Jet-Model-1} = 10\log\left[K_{Jet-model-1}^{empirical}\right] + DI(\theta) \tag{6}$$

The term $c_{Jet-Model-1}$ would remain the same for all the conditions, since θ and the system under study will not be changing. Since the underlying values for $c_{Jet-Model-1}$ are not known, initially, the SPL values will be computed in the absence of $c_{Jet-Model-1}$:

$$SPL_{Jet-Model-1}^{Basic} = 10\log\left[\frac{\rho_{Jet} v_{Jet}^8 D_{Jet}^2}{c_0^5 10^{-12}}\right] + 10\log\left[\frac{Q_{Jet}}{4\pi r^2}\right] \tag{7}$$

Once $SPL_{Jet-Model-1}^{Basic}$ values are obtained, $c_{Jet-Model-1}$ will be estimated by computing the mean offset between $SPL_{Jet-Model-1}^{Basic}$ and $SPL_{Jet(i)}^{experimental}$, that is:

$$\begin{aligned} &c_{Jet-Model-1} \\ &= \frac{1}{n}\sum_{i=1}^{n}[SPL_{Jet}^{experimental}(i) - SPL_{Jet-Model-1}^{Basic}(i)] \end{aligned} \tag{8}$$

where 'i' is the dataset number and 'n' is the total number of observations made during the experimentation (n =64).

Eventually, Jet Model 1 response will be computed by using the following relationship:

$$SPL_{Jet-Model-1} = SPL_{Jet-Model-1}^{Basic} + c_{Jet-Model-1} \tag{9}$$

Another model for jet noise estimation is also considered. This model is acquired from [20] which describes the acoustically radiated jet noise power to be dependent on the jet's mechanical power and its simplified version is given by:

b: JET MODEL 2

$$\begin{aligned} SPL_{Jet-Model-2}^{Basic} &= 10\log\left[C\frac{T_{Jet}^9}{T_{Amb}^2}\frac{\dot{m}_{MufflerExit}^8}{P_{Amb}^7}\right] \\ &+10\log\left[\frac{Q_{Jet}}{4\pi r^2}\right] \\ &+10\,log\left[K_{Jet-model-2}^{empirical}\right] + DI(\theta) \end{aligned} \tag{10}$$

where the term C is a comprised of several constant parameters,

$$C = \frac{\pi D_{Jet}^2 R^7}{c_0^5 A_{Jet}^8 8x10^{-12}}$$

And, $K_{Jet-model-2}^{empirical} = 5x10^{-5}$ for subsonic jets [20]. Since this model is also being evaluated for an APU first time, its deviation from the reference values will be recorded and corrections will be made in the model's output, that is:

$$SPL_{Jet-Model-2} = SPL_{Jet-Model-2}^{Basic} + c_{Jet-Model-2} \tag{11}$$

where, $c_{Jet-Model-2}$ will be computed in the same manner as in Eq. 8. This constant will accommodate for the differences between the model results and the experimental data.

2) COMBUSTION NOISE ESTIMATION MODELS

For the combustion noise estimation, SAE [21] and NASA [30] models are separately implemented. The SAE combustion model only relies on the thermodynamic parameters, whereas NASA's model also incorporates the geometrical parameters [Eq 13 and 12].

a: COMBUSTION MODEL 1

$$\begin{aligned} SPL_{C-Model-1}^{Basic} &= 10\log \\ &\times\left[\frac{\dot{m}_{Core}^4 T_{TurbineInlet}^2 F_b^2 4F}{A_b^2 P_3^2 N_f (1+F)^2}\left[1+\frac{H_f F_{st}}{c_p T_3}\right]^2\right] \\ &+10\log\left[\frac{Q_{Combustion}}{4\pi r^2}\right] + DI(\theta) + 131.3 \end{aligned} \tag{12}$$

where, $F = \frac{P_{TurbineInlet}}{P_{Amb}}\sqrt{\frac{T_{Amb}}{T_{TurbineInlet}}}$

b: COMBUSTION MODEL 2

$$SPL^{Basic}_{C-Model-2} = 10\log\left[\frac{\dot{m}_{Core}c_0^2}{10^{-12}}\left(\frac{T_{TurbineInlet}-T_3}{T_{TurbineInlet}}\right)^2 \left(\frac{P_3}{P_{Amb}}\right)^2\left(\frac{T_{TurbineInlet}-T_{Turbineexit}}{T_{Amb}}\right)^{-4}\right] + DI(\theta) - 60.5 + 10\log\left[\frac{Q_{Combustion}}{4\pi r^2}\right] \quad (13)$$

The Directivity Index (DI) in the above equations covers the variation in sound levels due to the angular placement of the sensor with respect to the source. This index is generally presented in tabulated form and the value is noted for $\theta = 60$ degrees to the jet axis. Furthermore, 'r' is the radial distance between the exhaust and the microphone.

Similar to the approach adopted for the jet noise models, the original form of the combustion noise models will be implemented and their results will be compared against $SPL^{experimental}_{Combustion}$ for possible offset computation. The corrected SPL values would become:

$$SPL_{C-Model-X} = SPL^{Basic}_{C-Model-X} + c_{C-Model-X} \quad (14)$$

where,

$$c_{C-Model-X} = \frac{1}{n}\sum_{i=1}^{n}[SPL^{experimental}_{Combustion}(i) - SPL^{Basic}_{C-Model-X}(i)] \quad (15)$$

$x = 1$ or 2 for Combustion noise model 1 and 2 respectively, 'i' is the dataset number and n =64.

Ideally, the constants $c_{Jet-Model-2}, c_{C-Model-1}$ and $c_{C-Model-2}$ should be zero, which would mean that the predicted results exactly match the measured values for the exhaust noise. However, this situation is unlikely to occur since these models are being evaluated for an aircraft APU for the first time, and there will be various inaccuracies inherent with the models, the directivity index, and the estimated thermodynamic parameters.

G. MODELING OF GROUND REFLECTIONS

A term Q is also embedded in the noise estimation models, that relate to the change in the sound levels due to the multi-path propagation of the sound. This term should take into consideration a number of factors that can affect the acoustic noise levels reaching the sensor. To find a relationship between those parameters, the reflection process is analytically studied, and an equation is subsequently derived. Consider a source of noise s(t) and its corresponding reflection reaching the microphone after Δ t seconds,

$$s_{rec}(t) = s(t) + c_{refl}s(t-\Delta t) \quad (16)$$

where, c_{refl} is the average value of the reflection coefficient of the surface. The frequency-domain representation would be:

$$s(t) + c_{refl}s(t-\Delta t) \rightarrow X(f) + c_{refl}X(f)\,e^{-j2\pi f\Delta t}$$

$$X(f) + c_{refl}X(f)\,e^{-j2\pi f\Delta t} = X(f)\left[1 + c_{refl}e^{-j2\pi f\Delta t}\right]$$

The second term in the above equation will modify the amplitude of the X(f), and will be termed as Q,

$$Q = E\left|1 + c_{refl}e^{-j2\pi f\Delta t}\right| \quad (17)$$

where E is the expected value operator. The above equation and its corresponding time-domain signal will become,

$$X(f)\,Q \rightarrow Qs(t)$$

This means that the addition of an indirect source of noise due to the ground reflection would modify the amplitude of the signal in the time domain. In order to compute the factor Q, the expected value of $\left|1 + c_{refl}e^{-j2\pi f\Delta t}\right|$ is computed in the following manner,

$$\begin{aligned}&\left|1 + c_{refl}e^{-j2\pi f\Delta t}\right| \\ &= |1 + c_{refl}\cos(2\pi f\Delta t) - jc_{refl}\sin(2\pi f\Delta t)| \\ &= \sqrt{(1 + c_{refl}\cos(2\pi f\Delta t))^2 + c_{refl}^2\sin^2(2\pi f\Delta t)} \\ &= \sqrt{1 + c_{refl}^2 + 2c_{refl}\cos(2\pi f\Delta t)}\end{aligned}$$

So, equation 17 becomes,

$$Q = \int_{f1}^{f2}\sqrt{1 + c_{refl}^2 + 2c_{refl}\cos(2\pi f\Delta t)}\,p(f)\,df$$

The probability density function $p(f)$ is uniform and is given by $p(f) = \frac{1}{f2-f1}$, so

$$Q = \frac{1}{f2-f1}\int_{f1}^{f2}\sqrt{1 + c_{refl}^2 + 2c_{refl}\cos(2\pi f\Delta t)}\,df \quad (18)$$

And,

$$s_{rec}(t) = s(t)\,\frac{1}{f2-f1}\int_{f1}^{f2}\sqrt{1 + c_{refl}^2 + 2c_{refl}\cos(2\pi f\Delta t)}\,df \quad (19)$$

According to the above relationship, the received signal's amplitude will be modified by a factor that is dependent on the value of the reflection coefficient, the time delay between the direct and indirect source of the sound, and the selected frequency range. This relationship will be utilized for estimating the term Q and the results will be presented in Section III.C.

The total sound pressure level at location M1 will be due to the contribution of the combustion and the jet noise. The addition of these noise sources is assumed to be non-coherent and is given by,

$$SPL_{Total} = 10\log\left[10^{[0.1(SPL_{C-Model-X})]} + 10^{[0.1(SPL_{Jet-Model-Y})]}\right] \quad (20)$$

where $\boldsymbol{X}$ and $\boldsymbol{Y}$ can be either 1 or 2 depending on the selected model.

III. RESULTS AND DISCUSSION

This section presents the outcomes of the developed noise estimation methodology which has been successfully implemented for the assessment of the B737 APU far-field noise. In this paper, the focus has been on the development of a thermodynamic model and its integration with the appropriate semi-empirical relationships for noise estimation. The former category of modelling can be treated independently and therefore its results will be presented first. The rationality of the results will be discussed based on the available literature and physics-based principles. The remaining part of the result section will present the outcomes of the noise estimation model. The acquired estimates are compared with the component level noise extracted using the frequency-domain technique. Finally, the total noise estimation models' results are presented and corroborated against the experimental data.

A. APU THERMODYNAMIC MODEL RESULTS

In this section, the acquired results from the thermodynamic simulation model are discussed which allow systematic assessment of the APU thermodynamics performance characteristics under a wide range of operating conditions (i.e. C1 – C8). To start with, the solver is converging to a point where all the constraints are met for all the 64 instances of the dataset. Convergence is reached as the solver iterates through various combinations of core mass flow and component efficiencies so that the measured EGT is reached, there is no shaft acceleration and the pressure at the diffuser exit equals the ambient pressure. The turbine inlet temperature is predicted to be a maximum at the bleed on conditions, shown in Fig. 8, with the values reaching as high as 816°C. As per [31], radial turbines can withstand such a level of temperatures for prolonged durations of operation. The acquired efficiency values (assumed to be maintained equal for both the compressor and the turbine) are estimated to be realistic for radial-type compressors and turbines [32] (Fig. 9).

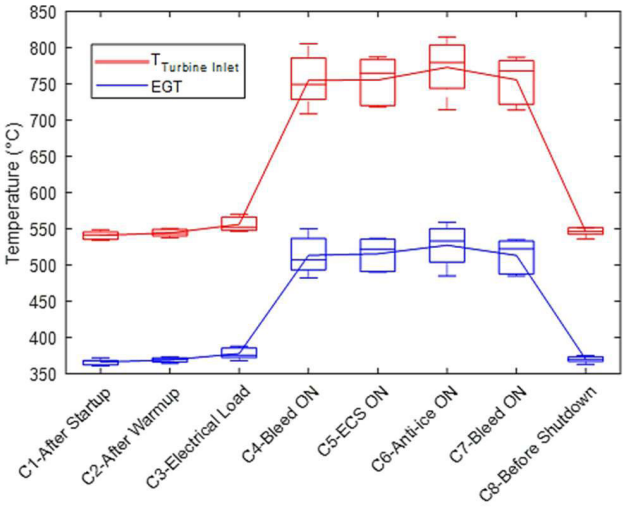

FIGURE 8. Measured EGT and estimated values of turbine inlet temperature.

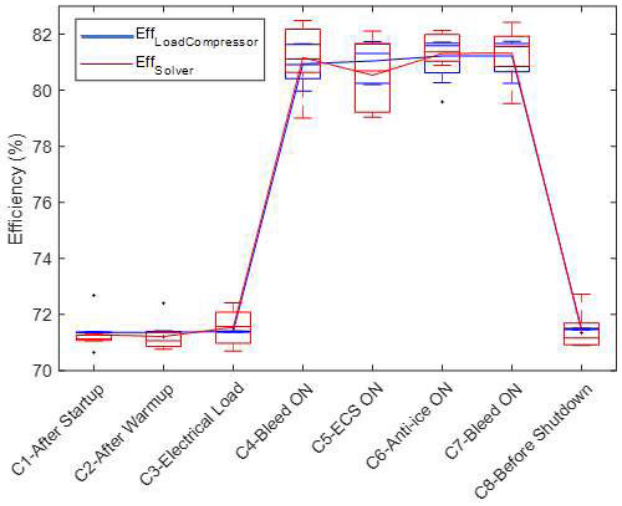

FIGURE 9. Component efficiencies for different operating conditions.

The thermodynamic results presented so far have been focused on the validity of various parameters related to the core of the APU, and are found to be acceptable, as they adhere to the first principles and engineering of the APU design and operation. In addition to the core parameters, the mass flow values corresponding to the surge control valve and the aircraft pneumatic system must also be determined and assessed. These two parameters are presented in Fig. 10.

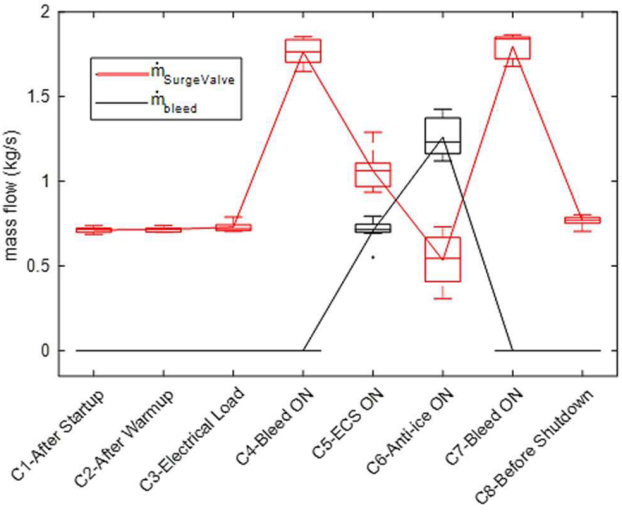

FIGURE 10. Comparison of mass flow through surge and the aircraft pneumatic system.

The results for the conditions (C1-C4 and C7-C8) are well estimated by the model, as under these conditions there is no pneumatic load and the entire mass flow generated by the load compressor must flow through the surge control valve. For condition-5 which corresponds to ECS ON, the verification of the mass flow values is carried out based on the data collected from the same aircraft Environmental Control System as part of a sister project [33], [34]. Lastly, the values for

C6 are based on the extrapolation of mass flow readings as a function of the surge control valve torque motor current. This produces a maximum flow rate of 1.42 kg/s through the aircraft pneumatic system when the anti-ice system is turned on. As per the aircraft manual, this reading is found to be less than the specified range of the APU bleed system and indicates that more mass flow can be provided by the APU by further closing the surge valve in case of higher pneumatic demand (e.g. main engine start).

B. DERIVED APU THERMODYNAMIC PARAMETERS

In this section, various derived thermodynamic parameters are presented that have been computed using thermodynamic principles. The focus will be on those parameters that present a strong influence on combustion and jet noise as per the literature. These include core mass flow, combustion inlet temperature, fuel to air ratio, mass flow and temperature across the muffler, and jet exit velocity. Figure 11 presents the first three parameters. During the high load conditions, the core mass flow decreases while the fuel to air ratio increases by 58-90% depending on the opening angle of the load compressor IGV. Furthermore, the combustor inlet temperature drops down by 30°C [Fig. 11(c)] during the full load conditions due to the increasing levels of isentropic efficiency.

With regards to the jet exit velocity, in terms of the APU, this requires an understanding of the mass flowing through the exhaust muffler. The APU exhaust flow is composed of (i) core mass flow, (ii) the flow coming through the surge control valve, and (iii) the cold mass flow added into the exhaust muffler through aspiration, (see Fig. 5). To begin with, a value of the factor 'F' has to be computed that controls the amount of the cold flow entering the muffler. The measured values of the muffler exit temperature have been chosen as a reference to select an appropriate value of F, such that the estimated results closely resemble the measured exit temperature.

The measurements of the exit temperature were taken during one of the test runs and are tabulated in Table 2. The estimated muffler exit temperature values correspond to 8% of the cold mass flow relative to the muffler inlet mass flow. Across all conditions, the cold mass flow is found to be varying between 0.24 – 0.36 kg/s, as shown in Fig. 12. The lowest value of $\dot{m}_{core}$ occurs at C6 when there is a drop in $\dot{m}_{SV}$ and $\dot{m}_{core}$. In this condition, the dynamic pressure at the muffler entrance will be reduced leading to a higher static pressure as compared to the other conditions. Consequently, the pressure difference across the muffler orifice will be reduced, which controls the amount of $\dot{m}_{cold}$ entering the muffler. The average temperature drop across the muffler due to the mixing of the cold mass flow with the APU hot exhaust flow is observed to be 26°C.

Under no-load conditions (C4 and C7), all the mass flow from the load compressor merges with the exhaust gases, thus lowering the temperature at the APU exit. The change in temperatures has an inverse effect on the flow densities. The performance parameters in terms of temperature, mass flow, density, and exit velocity for the APU exhaust and the muffler exit are presented in Fig. 13. The APU exit temperature is estimated to have a maximum value of 485°C which corresponds to ani-tice on conditions, being the highest demand from the APU. This condition leads to a reduction of mass flow from the APU bleed system (which is at a lower temperature) merging with the APU exhaust gases from the turbine (Fig. 10), thus leading to higher values of temperature.

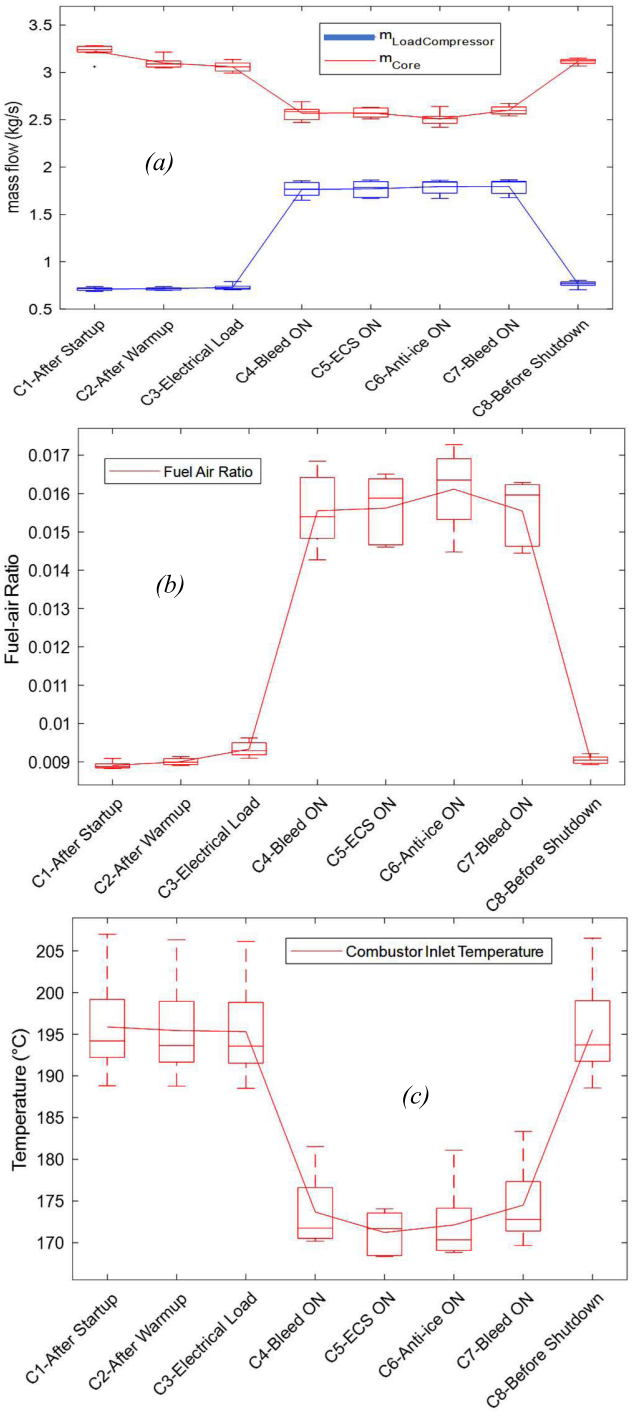

FIGURE 11. Derived engine parameters (a) core mass flow (b) Fuel air ratio (c) Combustor inlet temperature.

TABLE 2. Comparison of estimated and measured muffler exit temperature.

Load Condition	Estimated Muffler Exit Temp (°C)	Measured Muffler Exit Temp (°C)
No Load	293.5	300
Bleed ON	365	360
Anti-ice ON	450.6	450

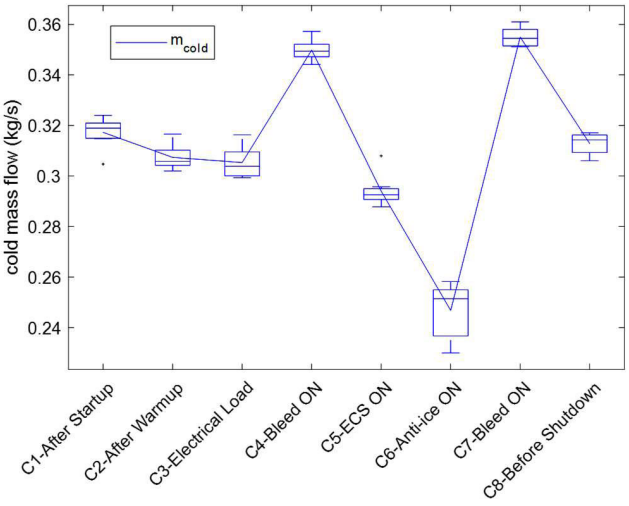

FIGURE 12. Estimated mass flow entering the muffler during various APU operating conditions.

The highest values for the exhaust mass flow and the exit velocity occur for C4 and C7, due to the increased level of mass flow from the load compressor. However, they are reduced when there is pneumatic power demanded from the aircraft (C5 and C6). The addition of a muffler leads to a slight increase in the mass flow and density while reducing the temperature and velocity which is significantly reduced mainly because of the increase in the duct diameter by 25%.

C. COMPONENT LEVEL NOISE SEPARATION RESULTS

This section will present the outcomes of the source separation technique applied to the far-field noise data. The complete process has already been described in Section II.E. Figure 14 shows the combustion and jet noise levels obtained from the far-field noise against all the 64 instances.

Following inferences can be made by observing the results:

1) The combustion and jet noise are approximately at the same levels when the bleed system is not operational.
2) The combustion noise increases when the bleed system is activated. The variation in this noise component within the bleed on conditions (dataset# 25-56) is because the IGVs behaved differently between different days of operation. For the cases where the IGV was fully opening, the fuel rate was observed to be high and correspondingly the combustion noise levels are also high.
3) The jet noise also increases with the bleed on conditions. This is because of the additional flow which is generated by the load compressor. This flow is proportional to the IGV opening angles and inversely proportional to the mass flow going through the surge valve. The conditions in which the aircraft pneumatic system is activated, there is a reduction in the flow exiting through the APU exhaust and therefore the jet noise decreases.

D. GROUND REFLECTION EFFECTS

In this section, the effect of ground reflections will be quantified based on the relationship derived in section II.G. To begin with, an experimental investigation of the far-field showed the presence of multiple equidistant nulls in the frequency spectrum (see Figure 15). Such a situation arises when the same source of sound is reaching the receiver through different paths. The far-field microphone has been placed inside a 6.5 cm diameter windscreen which raises the sensor by 3.25 cm above the ground. This seemingly small difference creates a time difference (Δt) of 78μs between the direct and the indirect source of noise using the geometrical parameters computed from the experimental setup (see Fig. 16). The time difference is computed after the values of distances 'a' and 'b' have been computed at which incidence and the reflected angles become equal. For validation of these results, the same Δt has been used to synthetically generate broadband noise and its delayed version for simulating reflections at the microphone. The results are shown in the frequency domain in Fig. 15 where the location of the nulls for synthetic data coincides with that of experimental data. It can also be seen that for certain frequencies the amplitude increases, whereas around the nulls the effect is opposite. Since the total noise is treated to be a combination of the combustion and the jet noise, a single value of Q is not valid for both and must be dependent on the frequencies of interest and the value of Δt.

To address the effect of ground reflection on the estimates of Combustion and Jet noise, the value of Q is found by solving Equation 18 for the desired set of parameters. The equation is solved numerically by using MATALB's *integral* function. Two different frequency ranges have been selected to account for the change in amplitudes occurring due to the ground reflections in the radiated combustion and the jet noise. For the former category of noise, frequencies are selected up to 2kHz since the combustion noise is dominant at those frequencies. For the jet noise, the integral is solved for the whole frequency range (0-25.6kHz), where the upper limit is determined by the selected sampling frequency. Using these frequency ranges and $c_{refl} = 0.97$ for the frequencies <2kHz and $c_{refl} = 0.93$ for the complete frequency range (these values are taken from [35] for concrete surface), the value of Q is computed to be 1.88 and 1.27 for the combustion noise and the jet noise, respectively.

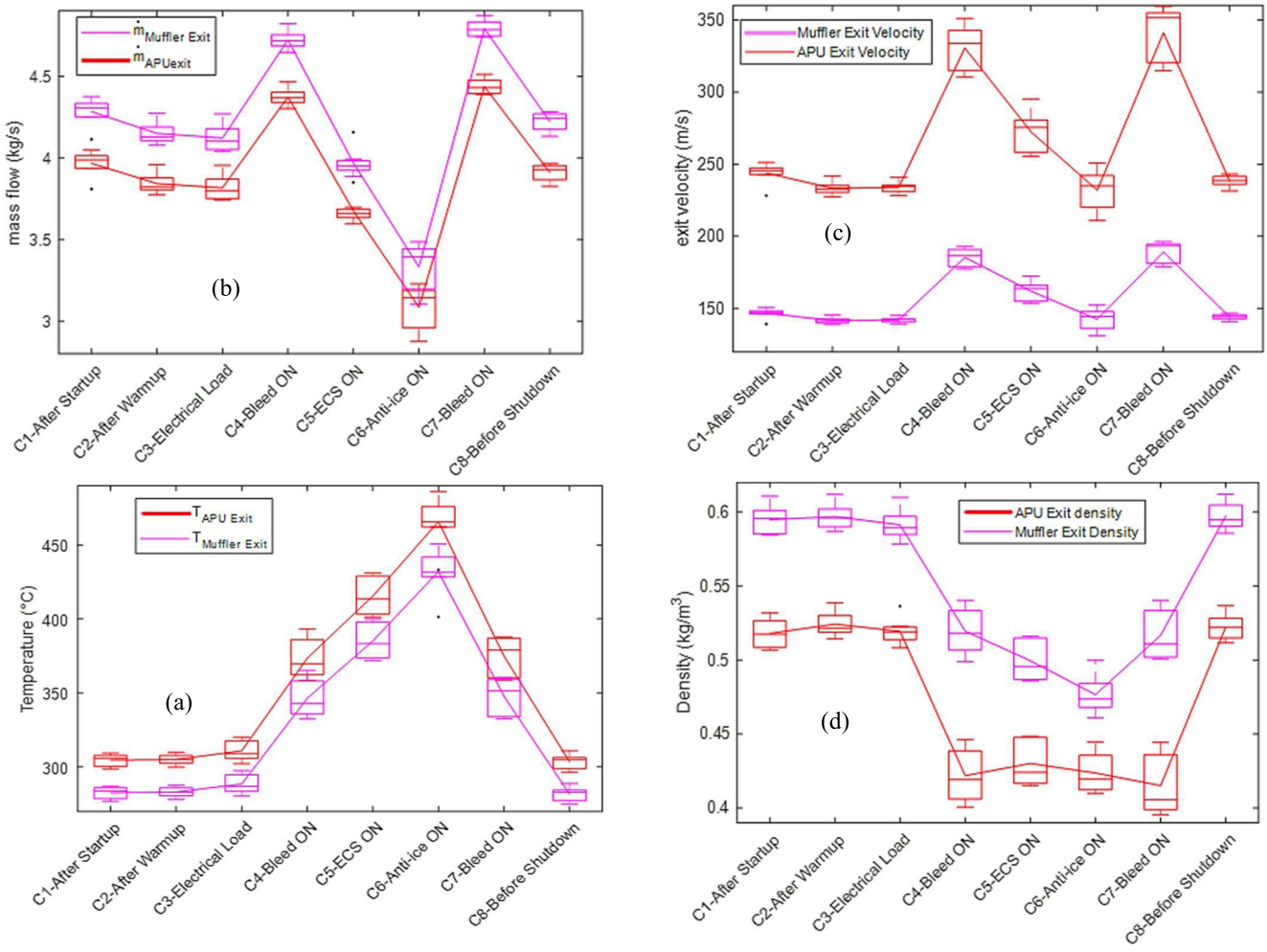

FIGURE 13. Estimated APU and muffler exit parameters.

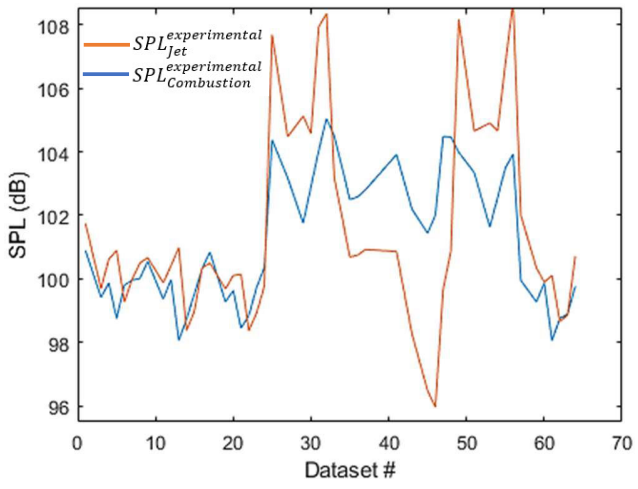

FIGURE 14. Noise source separation results.

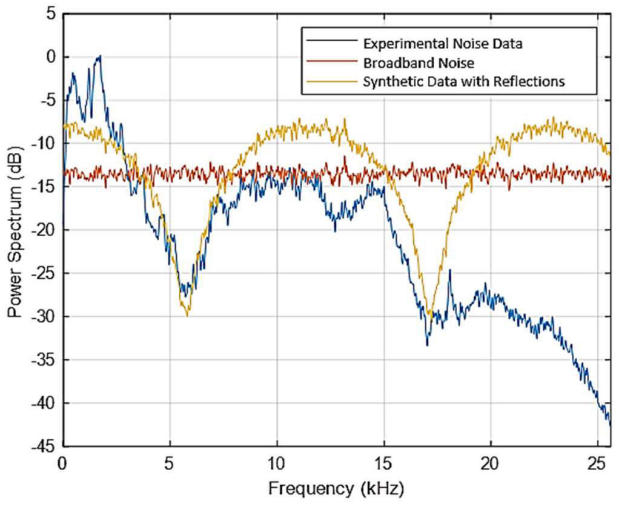

FIGURE 15. Comparison of experimental data and synthetically generated noise data with reflections.

E. NOISE ESTIMATION RESULTS

This section presents the acquired results for the APU noise estimation based on the implementation of the approach described in section II. The noise results in this section are presented for all the 64 datasets. Initially, the results of the individual noise estimation models (combustion and jet) will be discussed without computing the coefficients $c_{C-Model}$

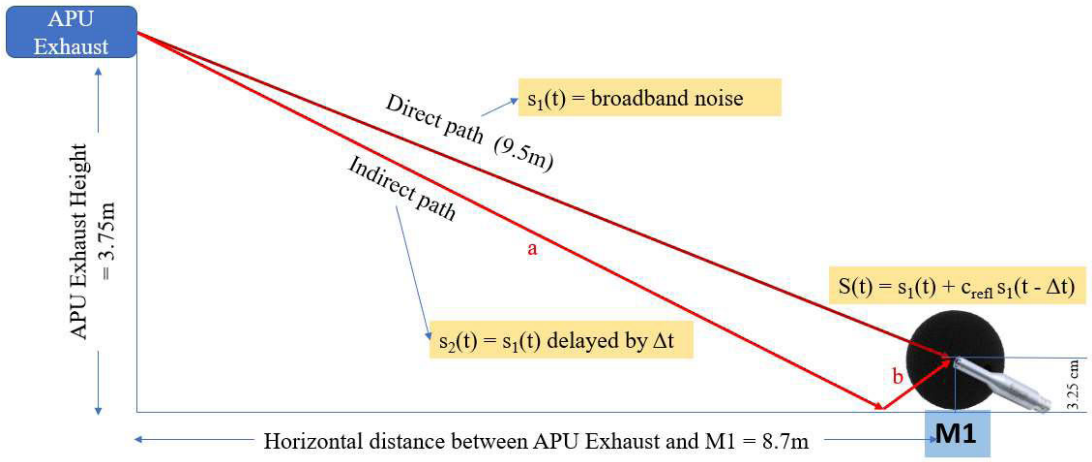

FIGURE 16. Vertical arrangement of the experimental setup and synthetic data generation for simulating ground reflections.

and $c_{Jet-Model}$ for each of the models. This is done to exclude any of the model(s) which does not corroborate well with the experimental data. Subsequently, those coefficients will be computed and lead to the estimation of the total far-field noise.

Considering the combustion noise first, the predicted results are shown in Fig. 17(a) for all the 64 instances of the dataset. These results are a direct outcome of the model's implementation, without applying the offset correction. As can be observed, the C-Model-2 demonstrates a very different behavior relative to C-Model-1 as well as $SPL^{experimental}_{Combustion}$ (see Fig. 14), both of which suggest an increase in the combustion noise levels during the bleed on conditions (Dataset # 25-54). Due to the dissimilar behaviour of C-Model-2, it will not be considered for further analysis. One of the reasons for the inappropriate behavior of C-Model-2 can be attributed to the fact that the number of underlying parameters included in the C-Model-2 is limited, and therefore the model is not robust enough to capture the variations taking place inside the combustor under a wide range of APU operating conditions.

The SPL values estimated from the two jet noise models are shown in Fig. 17(b). These values have been plotted without the offset correction. Both models behave similarly and follow the same pattern as in Fig. 14. Therefore, both jet noise models will be considered for further analysis and total noise computation. The extremely high value of noise computed from the Jet-Model-1 is because of the lack of information about $K^{empirical}_{Jet-model-1}$ and $DI(\theta)$ for this model.

To align the models' result with the experimental data, Eq. 8 and 15 has been employed to compute the coefficients $c_{Jet-Model-1}$, $c_{Jet-Model-2}$ and $c_{C-Model-1}$. These offsets are then applied to the basic forms of Jet-Model-1,2 and C-Model-1 so that, on average, their output matches $SPL^{experimental}_{Jet}$ and $SPL^{experimental}_{Combustion}$. C-Model-1 has been found to require the minimum offset (-0.48dB). This indicates

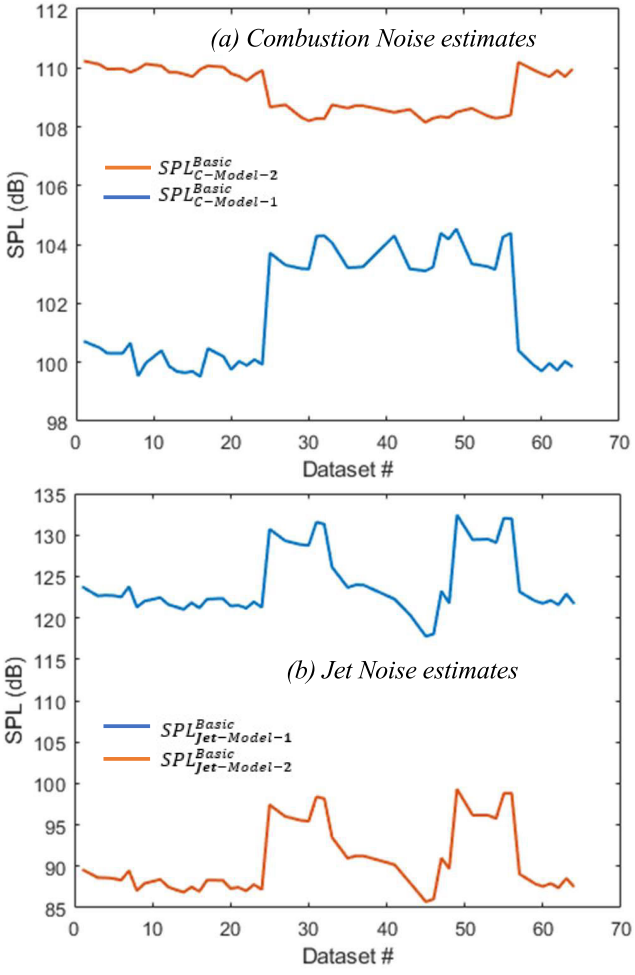

FIGURE 17. Estimated noise levels before offset correction.

that the overall accuracy of the estimated thermodynamic parameters and suitability of the C-Model-1 for an APU configuration presented in Fig. 1.

With regards to the jet noise models, a straightforward comparison between the computed offsets cannot be made. This is because for the Jet-Model-1, the computed offset ($c_{Jet-Model-1} = -23.6$dB using Eq. 8) covers the missing empirical coefficient and the Directivity Index. Whereas, for Jet-Model-2, the offset ($c_{Jet-Model-2} = 9.96$dB) is the correction to the original model. For comparison, all the empirical coefficients (including the offset for Jet-Model-2) can be combined in the following manner:

1) JET-MODEL-1

$$\text{Net effect of coefficients} = c_{Jet-Model-1} = -23.6\text{dB}$$

2) JET-MODEL-2

$$\begin{aligned}\text{Net effect of coefficients} &= 10\log\left[K^{empirical}_{Jet-model-2}\right] + DI(\theta) + c_{Jet-Model-2} \\ &= -26.05\text{dB}\end{aligned}$$

where, $K^{empirical}_{Jet-model-2}$ and $DI(\theta)$ are taken from [20]. For both the models, the overall effect of empirical coefficients is similar, and they are within 2.45dB of each other. Figure 18 shows the results of component-level noise estimation after the computed corrections have been applied. The combustion noise estimate can be seen to perform well under all the conditions [Fig. 18 (a)]. However, for the jet noise, there are discrepancies observed during certain conditions [Fig. 18(b)]. The results for the considered models are summarized in Table 3. The combustion model produces the most accurate reading with an RMS error of 0.69 dB. However, the jet noise estimates have RMS errors of 1.2dB and 1.52dB for models 1 and 2, respectively. The reason for the slightly higher level of inaccuracy for the jet noise can be attributed to the fact that a very large frequency spectrum (up to 25.6 kHz) is considered where minor contributions can also be taking place from other components which have not been considered. Amongst the jet noise models, Jet-Model-1 performs well than the other.

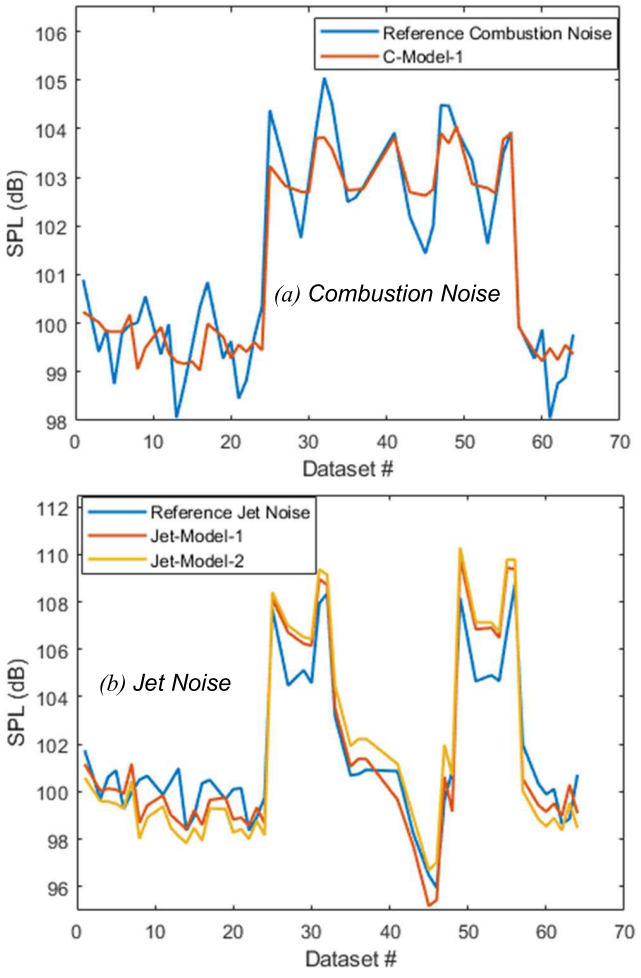

FIGURE 18. Comparison of estimated noise levels after offset corrections.

TABLE 3. RMS and maximum error for combustion and jet noise estimates.

Parameter (dB)	C-Model-1	Jet-Model-1	Jet-Model-2
Max Error	1.44	2.67	3.00
RMS Error	0.69	1.20	1.52

Finally, two sets of models are available for computing the total noise and validating their performance with the experimental data. These models employ Eq. 20 and are given by:

3) TOTAL NOISE MODEL 1 (TNM-1)

$$SPL_{TNM-1} = SPL_{C-Model-1}(+)SPL_{Jet-Model-1} \quad (21)$$

4) TOTAL NOISE MODEL 2 (TNM-2)

$$SPL_{TNM-2} = SPL_{C-Model-1}(+)SPL_{Jet-Model-2} \quad (22)$$

where, $(+)$ represents addition in dB scale.

In Fig. 19 the total noise level estimates from the (*TNM-1 and TNM-2*) are presented. The acquired estimated correlate well against the measured noise data ($SPL_{Measured}$) throughout the 64 instances, with the *TNM-1* (RMS error = 0.73 dB) being slightly better than its counterpart (RMS error = 0.85 dB). As per the analysis, the maximum deviation for the total noise estimation can be 1.30 dB and 1.56 dB for TNM-1 and TNM-2 respectively.

Following inferences can be drawn after observing the results:

1) Far-field noise from aircraft APU is dominated by combustion and jet noise. Correct estimation of these two components can allow accurate estimation of the total far-field noise.
2) There are a number of semi-empirical noise estimation models available in the literature. However, not all of them could be suitable for the desired category of a gas turbine. Some of these models are either restricted to

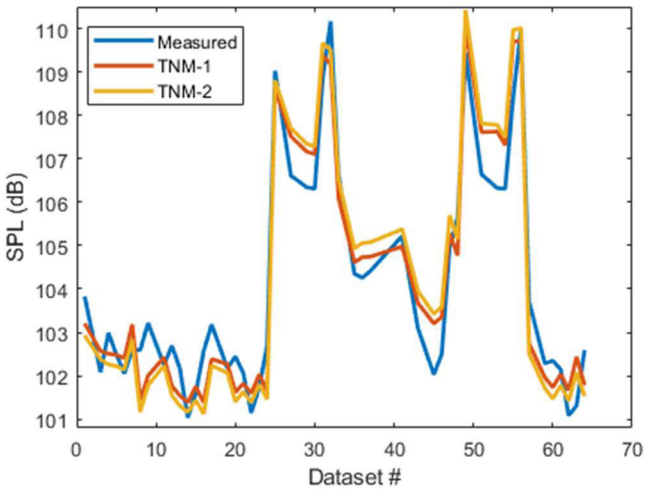

FIGURE 19. Total noise estimation results.

turbofan engines or they could be applicable to only one state of operation (like take-off condition). Careful selection of these models is needed by comparing the results from various models.

3) Accurate modeling of noise propagation is needed along with the estimation models. This model should cater to the decrease in noise power due to spherical divergence, ground reflections (or any other reflections taking place), and the effects of the selected frequency range on the reflections.
4) The gathering of a diverse set of APU noise and thermodynamic data by operating the APU in a range of different load conditions, allows the deviation between the model results and experimental data to be detected. This deviation can be used to compute the average value of offset that can bring the model output closer to the experimental data.
5) The correctness of the results indicates that the proposed framework is performing well under a wide range of conditions. This also ensures that the various assumptions made during the whole process are acting well within the overall integrated approach.

IV. CONCLUSION

In this paper, a methodology for the development of a far-field noise estimation model has been proposed and implemented on a Boeing 737-400 aircraft Auxiliary Power Unit (APU) during steady-state operations. The approach makes use of the open-source thermodynamic modelling package (Toolbox for the Modeling and Analysis of Thermodynamic Systems [T-MATS]) and recommends modification of its turbomachinery blocks to operate in the absence of the components' performance characteristics. The resultant thermodynamic parameters have been shown to exhibit logical behaviour under a wide range of operating conditions. Another contribution of this study is the evaluation of various noise estimation models for an aircraft APU, which have not been reported in the literature so far. Two combustion noise models and two jet noise models are considered for evaluation. These models have been integrated with the outputs of the thermodynamic model for examination. For comparing the noise models results, reference values of the combustion and jet noise are found by applying the source separation technique on the experimental far-field noise data. An immediate analysis reveals that one of the combustion estimation models is not in agreement with the experimental data and is therefore excluded from further analysis. In the case of jet noise, the models' output has to be scaled by a constant offset. After applying the corrections, the total noise estimation model can predict the far-field noise levels with a Root Mean Square Error of 0.73 dB.

The overall approach compiled is innovative and is useful for rapid estimation of thermodynamic parameters and the far-field noise from a limited parameter set. The approach will be subsequently capitalized by developing a standalone noise estimation model that would allow fault simulation and study of faults/degradations effects on the far-field noise.

ACKNOWLEDGMENT

The authors would like to thank Cengiz Turkoglu (a Senior Lecturer at the Safety Engineering Centre, Cranfield University) for providing his expert support in aircraft experimentation and data collection.

REFERENCES

[1] C. Skliros, F. Ali, and I. Jennions, "Experimental investigation and simulation of a boeing 747 auxiliary power unit," *J. Eng. Gas Turbines Power*, vol. 142, no. 8, Aug. 2020, Art. no. 081005, doi: 10.1115/1.4047771.
[2] T. Siebel, J. Zanger, A. Huber, M. Aigner, K. Knobloch, and F. Bake, "Experimental investigation of cycle properties, noise, and air pollutant emissions of an APS3200 auxiliary power unit," *J. Eng. Gas Turbines Power*, vol. 140, no. 6, pp. 1–9, Jun. 2018, doi: 10.1115/1.4038159.
[3] J. Zanger, T. Krummrein, T. Siebel, and J. Roth, "Characterization of an aircraft auxiliary power unit test rig for cycle optimization studies," *J. Eng. Gas Turbines Power*, vol. 141, no. 1, pp. 1–9, Jan. 2019, doi: 10.1115/1.4041119.
[4] S. A. D. Wiesche, "A mobile test rig for micro gas turbines based on a thermal power measurement approach," *J. Eng. Gas Turbines Power*, vol. 134, no. 11, pp. 467–477, Nov. 2012, doi: 10.1115/1.4007201.
[5] C. K. Tam, "On the spectrum of combustion noise," in *Proc. 21st AIAA/CEAS Aeroacoustics Conf.*, Jun. 2015, p. 2969, doi: 10.2514/6.2015-2969.
[6] C. K. W. Tam, S. A. Parrish, J. Xu, and B. Schuster, "Indirect combustion noise of auxiliary power units," *J. Sound Vib.*, vol. 332, no. 17, pp. 4004–4020, Aug. 2013, doi: 10.1016/j.jsv.2012.11.013.
[7] B. N. Shivashankara, "Gas turbine core noise source isolation by internal-to-far-field correlations," *J. Aircr.*, vol. 15, no. 9, pp. 597–600, Sep. 1978, doi: 10.2514/3.58412.
[8] K. Knobloch, L. Enghardt, and F. Bake, "APU-noise reduction by novel muffler concepts," in *Proc. ASME Turbo Expo*, 2018, pp. 1–11, doi: 10.1115/GT2018-76762.
[9] M. Pott-Pollenske, W. Dobrzynski, H. Buchholz, and D. Almoneit, "Characteristics of noise from aircraft ground operations," in *Proc. 13th AIAA/CEAS Aeroacoustics Conf.*, May 2007, pp. 1–14, doi: 10.2514/6.2007-3560.
[10] R. L. Tubbs, "Case studies noise exposure to airline ramp employees," *Appl. Occupational Environ. Hygiene*, vol. 15, no. 9, pp. 657–663, Jan. 2000, doi: 10.1080/10473220050110022.
[11] F. Gugliermetti, F. Bisegna, A. C. Violante, and C. Aureli, "Noise exposure of the ramp's operators in airport apron," in *Proc. 20th Int. Congr. Acoust.*, vol. 3, Aug. 2010, pp. 2051–2057.

[12] A. Filippone, "Aircraft noise prediction," *Prog. Aerosp. Sci.*, vol. 68, pp. 27–63, Jul. 2014, doi: 10.1016/j.paerosci.2014.02.001.
[13] M. Harper-Bourne, A. Moore, and H. Siller, "A study of large aero-engine combustor noise," in *Proc. 14th AIAA/CEAS Aeroacoust. Conf.*, May 2008, p. 2942, doi: 10.2514/6.2008-2942.
[14] G. Podboy and C. Horvath, "Phased array noise source localization measurements made on a Williams international FJ44 engine," in *Proc. 15th AIAA/CEAS Aeroacoustics Conf.*, May 2009, pp. 11–13, doi: 10.2514/6.2009-3183.
[15] D. K. Boyle, B. S. Henderson, and L. S. Hultgren, "Core/combustor-noise baseline measurements for the DGEN aeropropulsion research turbofan," in *Proc. AIAA/CEAS Aeroacoustics Conf.*, Jun. 2018, pp. 25–29, doi: 10.2514/6.2018-3281.
[16] H. Gounet and S. Lewy, "Three-dimensional sound directivity around a helicopter turboshaft engine," *J. Amer. Helicopter Soc.*, vol. 57, no. 4, pp. 1–10, Oct. 2012, doi: 10.4050/JAHS.57.042002.
[17] J. Mendoza, D. Nance, and K. Ahuja, "Source separation from multiple microphone measurements in the far field of a full scale aero engine," in *Proc. 14th AIAA/CEAS Aeroacoust. Conf.*, May 2008, pp. 1–7, doi: 10.2514/6.2008-2809.
[18] R. Otero, K. T. Lowe, W. Ng, L. Ma, and C. Kim, "Non-intrusive measurement of gas turbine engine exhaust characteristics using acoustic measurements," in *Proc. 32nd AIAA Aerodyn. Meas. Technol. Ground Test. Conf.*, Jun. 2016, pp. 1–13, doi: 10.2514/6.2016-4160.
[19] U. Ahmed, F. Ali, and I. Jennions, "A review of aircraft auxiliary power unit faults, diagnostics and acoustic measurements," *Prog. Aerosp. Sci.*, vol. 124, Jul. 2021, Art. no. 100721, doi: 10.1016/j.paerosci.2021.100721.
[20] M. Munjal, "Noise control strategies," in *Noise and Vibration Control* (IISc Lecture Notes Series), vol. 3. Bangalore, India: IISc Press, 2013, pp. 221–266.
[21] *Gas Turbine Jet Exhaust Prediction*, document ARP876F, SAE 2013.
[22] B. Yu, C. Cao, W. Shu, and Z. Hu, "A new method for the design of optimal control in the transient state of a gas turbine engine," *IEEE Access*, vol. 5, pp. 23848–23857, 2017, doi: 10.1109/ACCESS.2017.2764056.
[23] J. W. Chapman, T. M. Lavelle, R. May, J. S. Litt, and T.-H. Guo, "Propulsion system simulation using the toolbox for the modeling and analysis of thermodynamic systems (T MATS)," in *Proc. 50th AIAA/ASME/SAE/ASEE Joint Propuls. Conf.*, Jul. 2014, p. 3929, doi: 10.2514/6.2014-3929.
[24] A. Baylar, F. Ozkan, and M. Unsal, "Effect of air inlet hole diameter of venturi tube on air injection rate," *KSCE J. Civil Eng.*, vol. 14, no. 4, pp. 489–492, Jul. 2010, doi: 10.1007/s12205-010-0489-6.
[25] B. Khandelwal, "Development of gas turbine combustor preliminary design methodologies and preliminary assessments of advanced low emission combustor concepts," Cranfield Univ., Bedford, U.K., Tech. Rep. 2015-03-05T17:06:45Z, 2012.
[26] *Gas Turbine Combustion Efficiency*, document IGT-121, ASME, 1985.
[27] B. Schuster and L. Lieber, "Narrowband model for gas turbine engine combustion noise prediction," in *Proc. 12th AIAA/CEAS AeroAcoust.*, vol. 6, May 2006, pp. 3611–3623, doi: 10.2514/6.2006-2677.
[28] H. Schmid, "How to use the FFT and MATLAB's pwelch function for signal and noise simulations and measurements," Univ. Appl. Sci., Cham, Switzerland, Tech. Rep. FHNW/IME, Aug. 2012.
[29] J. R. Barbosa and D. J. Dezan, "Single-stream jet noise prediction using empirical methodology for a newly designed turbojet engine," *Proc. ASME Turbo Expo*, vol. 2, Nov. 2014, pp. 1–5, doi: 10.1115/GT2013-95199.
[30] J. W. Rawls and J. C. Yeager, "High speed research noise prediction code (HSRNOISE) user's and theoretical manual," NASA, Richmond, VA, USA, Tech. Rep. Nasa/Cr-2004-213014, Nov. 2004.
[31] A. F. El-Sayed, "Fundamentals of aircraft and rocket propulsion," Blackwell Sci., London, U.K., Tech. Rep., 2016, doi: 10.1007/978-1-4471-6796-9.
[32] P. Fletcher and P. P. Walsh, *Gas Turbine Performance*, vol. 1. 2004, pp. 159–291.
[33] I. Jennions and F. Ali, "Assessment of heat exchanger degradation in a boeing 737-800 environmental control system," *J. Thermal Sci. Eng. Appl.*, vol. 13, no. 6, pp. 1–13, Dec. 2021, doi: 10.1115/1.4050324.
[34] S. H. Chowdhury, F. Ali, and I. K. Jennions, "A methodology for the experimental validation of an aircraft ECS digital twin targeting system level diagnostics," *Proc. Annu. Conf. Progn. Heal. Manag. Soc.*, vol. 11, no. 1, pp. 21–26, 2019, doi: 10.36001/phmconf.2019.v11i1.888.
[35] M. Vorlander. (2007). *Material Data Absorption*. [Online]. Available: https://cds.cern.ch/record/1251519/files/978-3-540-48830-9_BookBackMatter.pdf

UMAIR AHMED received the bachelor's degree in avionics from the National University of Science and Technology, Islamabad, Pakistan, and the master's degree in avionics from Air University, Islamabad. He is currently pursuing the Ph.D. degree with Cranfield University. He has been working with IVHM Centre, since 2019. He has worked towards development of flight simulators for a period of four years. His role, being a Design Engineer, has been to design and develop software/hardware for integrating various sub-systems of a simulator. For three years, he has also been part of the Aviation Design Institute, where he was tasked to evaluate and integrate various avionics sub-systems. His current research interests include development of acoustic signal processing and machine learning techniques for fault detection of aircraft auxiliary power unit.

FAKHRE ALI received the degree in mechanical engineering and the Ph.D. degree (engineering) in aerospace propulsion from Cranfield University, U.K. He is currently a Research Fellow in simulation and test with IVHM Centre, Cranfield University. In his current role, he is responsible for the successful planning, implementation, and delivery of TRL four to five level projects, dedicated towards identifying new IVHM solutions for various major civil aircraft sub-systems i.e., APU and ECS. He is a Mechanical Engineer and a member of IMechE and RAeS.

IAN K. JENNIONS received the degree in mechanical engineering and the Ph.D. degree in CFD from Imperial College London, London.

His career spans over 40 years, working mostly for a variety of gas turbine companies. He has worked for Rolls-Royce (twice). He has worked at General Electric and Alstom in a number of technical roles, gaining experience in aerodynamics, heat transfer, fluid systems, mechanical design, combustion, services, and IVHM. In July 2008, he moved to Cranfield as a Professor and the Director of the newly formed IVHM Centre. The centre is funded by a number of industrial companies, including Boeing, BAE Systems, Thales, Meggitt, MOD, and Alstom Transport. He has led the development and growth of the centre, in research and education, since its inception. The centre offers an IVHM short course each year and has offered an IVHM M.Sc. He is the Editor of five recent SAE books, such as *IVHM: Perspectives on an Emerging Field*, *IVHM: Business Case Theory and Practice*, *IVHM: The Technology*, *IVHM: Essential Reading*, and *IVHM: Implementation and Lessons Learned*. He is the coauthor of the book *No Fault Found: The Search for the Root Cause*. He is the Director of PHM Society, the Vice-Chairman of SAE's IVHM Steering Group, a Contributing Member of the SAE HM-1 IVHM Committee, a Chartered Engineer, and a fellow of IMechE, RAeS, and ASME. He is on the Editorial Board for the *International Journal of Condition Monitoring*.